Fast vapour migration next to a depressurizing interface: A possible driving mechanism of explosive spalling revealed by neutron imaging

Roberto Felicetti, Ramin Yarmohammadian, Stefano Dal Pont, Alessandro Tengattini

Cement and Concrete Research 180 (2024) 107508

Contents lists available at ScienceDirect

Cement and Concrete Research

journal homepage: www.elsevier.com/locate/cemconres

Fast vapour migration next to a depressurizing interface: A possible driving mechanism of explosive spalling revealed by neutron imaging

Roberto Felicetti [a], Ramin Yarmohammadian [a,*], Stefano Dal Pont [b], Alessandro Tengattini [c]

[a] Politecnico di Milano, Milan, Italy
[b] Université Grenoble Alpes, Grenoble, France
[c] Institut Laue-Langevin, Grenoble, France

ARTICLE INFO

Keywords:
Fire-induced spalling
Concrete
Moisture content
Thermal energy
Neutron radiography

ABSTRACT

When exposed to high temperatures, concrete is prone to explosive spalling, resulting in the projection of concrete flakes and the reduction of the structural element cross-section. Elastic energy alone cannot justify the explosive nature of the process: accumulated thermal energy serves as a supplementary source, together with the water in the pores, which can generate kinetic energy through vaporization. The objective of this paper is to study the fast thermal and hygral transients occurring upon depressurization of an internal interface, emulating a crack developing in hot moist concrete. One possible mechanism that could justify this contribution is the flash vaporization of water. This paper presents a new experimental approach to directly measure flash vaporization through rapid-neutron imaging. Additionally, a thermo-hygral model assesses key parameters influencing fast-transient phenomena. Experimental observations reveal moisture loss in a 1-mm-thick layer, equating to a 90 °C temperature drop, justifying a significant amount of released energy.

1. Introduction

A broad body of research has extensively investigated the mechanical properties and durability of concrete as the most used structural material. Nonetheless, its predisposition to explosive spalling, when subjected to high temperatures, is often ignored or underestimated, being a not completely understood phenomenon. The term spalling refers to the detachment (violent or not) of layers from the surface of concrete elements exposed to high temperatures; this process reduces the working cross-section and can expose the reinforcement, leading to early partial or total structural failure [1,2].

This occurrence is driven by the complex coupling of thermo-hydro-mechanical processes and is still unclear at the fundamental level [3]. A factor known to play a key role is the stress induced by thermal dilation (Fig. 1-a) i.e., from thermal gradients [4,5] and the contribution coming from the restrain to thermal dilation exerted by the boundary conditions [6–10].

Another crucial factor is the increase of pore pressure induced by water evaporation (Fig. 1-b), measured first by Kalifa et al. [11]. In this and the ensuing works, the temperature and pressure were measured pointwise with embedded probes [12–14].

A doubt is nevertheless raised about the actual contribution of this pressure upon the opening of the crack that vastly increases the available volume [8]. The relative contribution of these components is still under debate by the community [15,16].

Later, Felicetti et al. performed splitting tests on cubic samples heated at high temperatures linearly correlating an increase in the measured pore pressure in the middle of the sample with a loss of tensile strength [18]. The systematic analysis of a series of concrete mixes [19]. revealed how in high-performance concrete only a minor fraction of pore pressure (about 25 %) translates into effective tensile stress, because of the low interconnectivity of the pores.

These works adopt pointwise or macroscopic measurements, which are limited given the intrinsic heterogeneity of the material as well as the invasiveness of some types of probes [20]. In recent works, non-destructive techniques have provided insight into moisture migration [21–23] in concrete proving that vapour can condense in colder regions altering locally the permeability (a process named “moisture clog”) and increasing the vapour pressure that could otherwise be sustainable. Nonetheless, in high-performance concrete, the measured pore pressure generally does not exceed 5 MPa in the temperature range (220–300 °C), where spalling is known to occur. Hence, the ensuing effective stress is far from the tensile strength, as also testified by the observation that slowly heated unloaded samples generally survive the heating process

* Corresponding author.
E-mail address: Ramin.yarmohammadian@polimi.it (R. Yarmohammadian).

https://doi.org/10.1016/j.cemconres.2024.107508
Received 26 September 2023; Received in revised form 25 March 2024; Accepted 3 April 2024

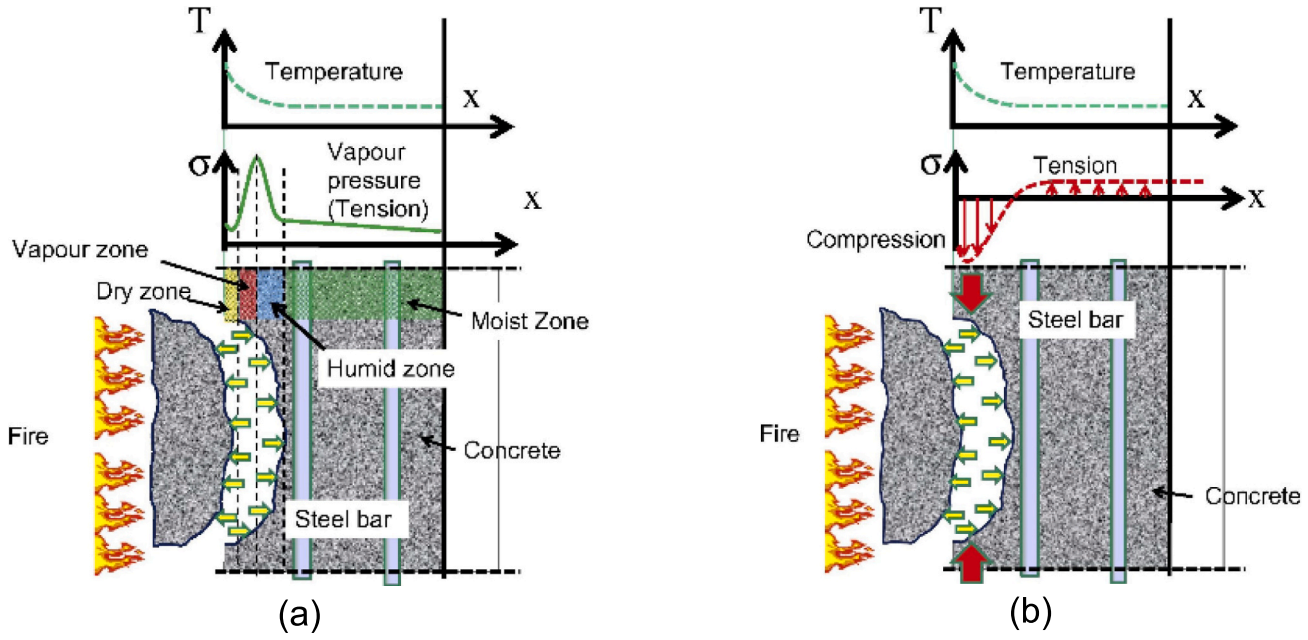

Fig. 1. Schematic of two mechanisms inducing spalling: (a) Thermal stress and (b) Pore pressure [11,17].

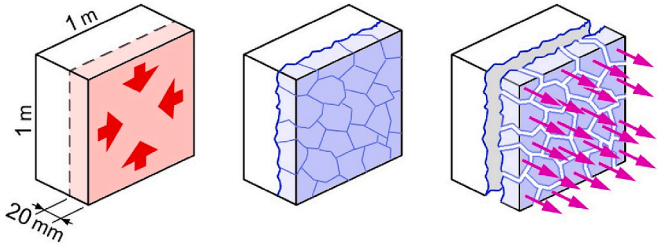

Fig. 2. Elastic strain energy accumulated in the hot cover and energy-demanding mechanisms entailed by spalling (fracturing and shard acceleration).

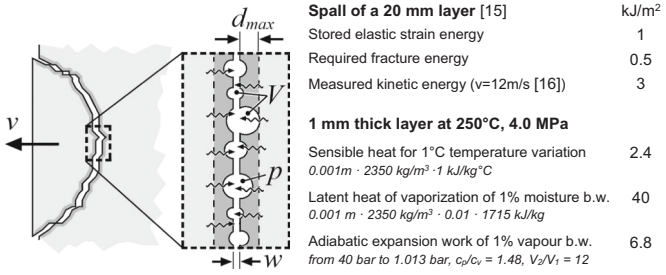

Fig. 3. The influencing region next to an opening crack [16] and magnitudes of involved energy contributions.

[19]. On the contrary, loaded or rapidly heated samples are more prone to fail explosively, proving the synergetic effect of pore pressure and thermal stress in triggering fractures [24].

The highly unstable crack propagation also suggests an insight into the energy balance driving the process [15,16,25]. A part of the provided energy is consumed for fracturing concrete into pieces, and the remaining part is instead transformed into kinetic energy (see Fig. 2).

One first balance was reported in numerical analysis by Gawin et al. [15] where they considered a concrete cover (20 mm) of a unit square meter which can accumulate elastic energy due to the thermal gradient (see Fig. 2) while the velocity of ejected fragments was later measured by Zeiml et al. using a high-speed camera [16]. It turned out that the elastic energy due to thermal stress is not sufficient to drive such an unstable fracture and a contribution from vapour expansion should be introduced.

On the other hand, some authors proved sceptical about the role of pore pressure in accelerating the fractured shards [8] because the opening of a crack implies a significative increase of the pore volume with little to no water flowing into this gap from the surrounding concrete. Then a sudden pressure drop is expected and, according to [8], only the elastic strain energy due to thermal stress would be converted into fracture and kinetic energy. Gawin et al. [15] proposed an energy balance suggesting that the contribution from pore pressure was necessary when the splinter velocity exceeds 5 m/s (as measured in [14]). According to the authors, the energy balance can be reached by considering the adiabatic expansion of an initial volume of pressurized vapour into a widely open crack (0.5 mm) filled with gas at significant pressure (4 MPa). However, such a steady condition is not realistic since concrete loses most of its tensile strength already with a tenfold thinner crack [26,36].

An alternative to account for the mechanical work developed by pressurized fluids was the definition of the “influencing region” [14], i.e. the thin layer around the crack contributing to the inflow of water vapour into the opening gap (Fig. 3). Though no indication was provided about the possible thickness of the influencing region, this is a key parameter, since the time required for moisture to flow towards the opening crack strongly depends on the path length (time in diffusion phenomena goes with the distance squared). Due to the low permeability of concrete, quick moisture migration and vaporization entail a very thin volume surrounding the crack. Because of the challenging experimental difficulties, this aspect has never been validated by way of specific experiments.

We attempt to study an aspect of these complex thermo-hydro-mechanical couplings by focusing on the role that the opening of a fissure has on the temperature and pressure drop and the possibility of an ensuing local flash vaporization. The idea herein proposed is to trigger this sudden drop of pore pressure on one face of a hot concrete sample by draining vapour from a sealed gap connected to a relief valve. Taking advantage of the high time and spatial resolution of the neutron and X-ray tomograph NeXT-Grenoble at the Institut Laue-Langevin [26], the local evolution of the moisture distribution in the region facing the

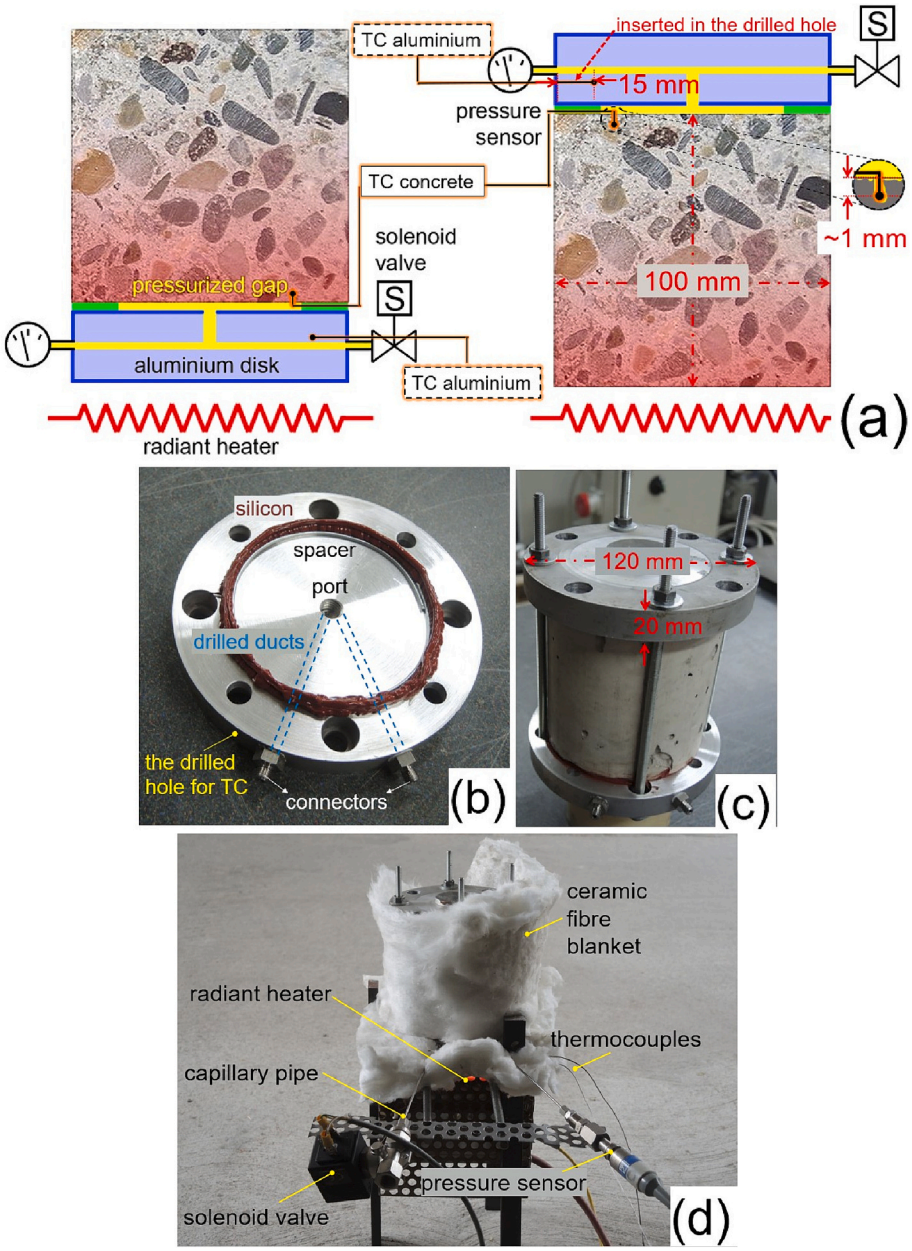

Fig. 4. First validation tests: (a) Two different schemes; (b,c) Sample's details; (d) Details of the setup.

gap could be monitored with a fast sequence of neutron radiographies during the transient. This allowed us to gain a deeper insight into the intriguing concept of the influencing region, with direct observation of its thickness and drying rate. The background idea, the test setup and some results are illustrated in the following sections. The results would allow us to clarify the role of moisture migration and vaporization in driving the dynamic fracture of spalling concrete. They would also represent a unique benchmark for tuning and validating advanced numerical models of the thermo-hygral transients developing in spalling concrete.

2. Aim of the experimental campaign

As discussed, the magnitude of the different energy shares governing the sudden separation of concrete fragments from the exposed cover was the object of former studies available in the literature [15,16]. Some indicative energy values per unit spalled area are reported in Fig. 3, together with the terms entailed by unit variations of temperature and moisture content within a layer of unit thickness under typical conditions for incipient spalling.

These latter values should be doubled since both faces of the opening crack are influenced by the concrete right behind them. What stands out is the dominant role of thermal energy and latent heat of vaporization compared to what is demanded for fracturing and accelerating the surface splinters. Cooling a thin layer of hot concrete by a few tens of degrees provides the energy required for vaporizing a significant amount of water contained in its pores (e.g. vaporization of 1 % moisture in 1 mm thickness corresponds to a latent heat of 40 kJ/m^2, i.e. a temperature drop of 16 °C, see Fig. 3). If one considers that the heat flux entering the exposed face of a concrete member during the first 10 min of severe fire scenarios (from standard to RWS fires) can be as high as 25–50 kW/m^2, the energy mobilized by explosive spalling corresponds to the thermal flux accumulated by the concrete cover in less than 1 s. Furthermore, the amount of water which should quickly vaporize and expand to accelerate the fractured shards to their maximum observed velocity can be taken from a layer much thinner than 1 mm, provided its

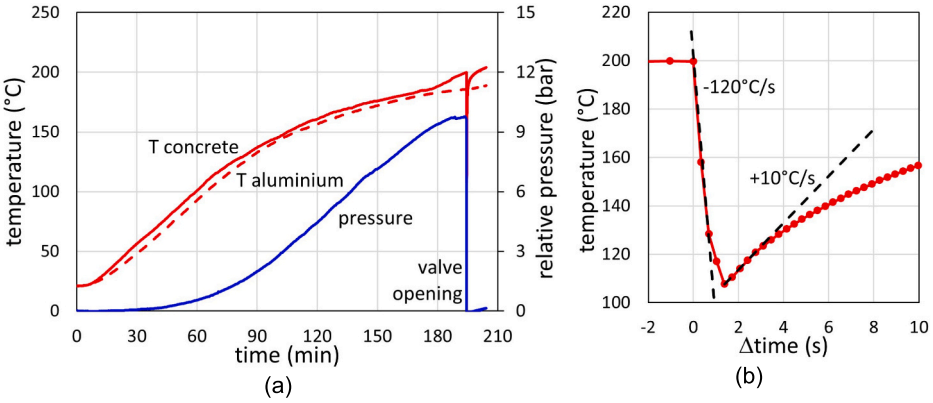

Fig. 5. (a)Temperature and (b) Pressure trends in a preliminary trial test (sealed face).

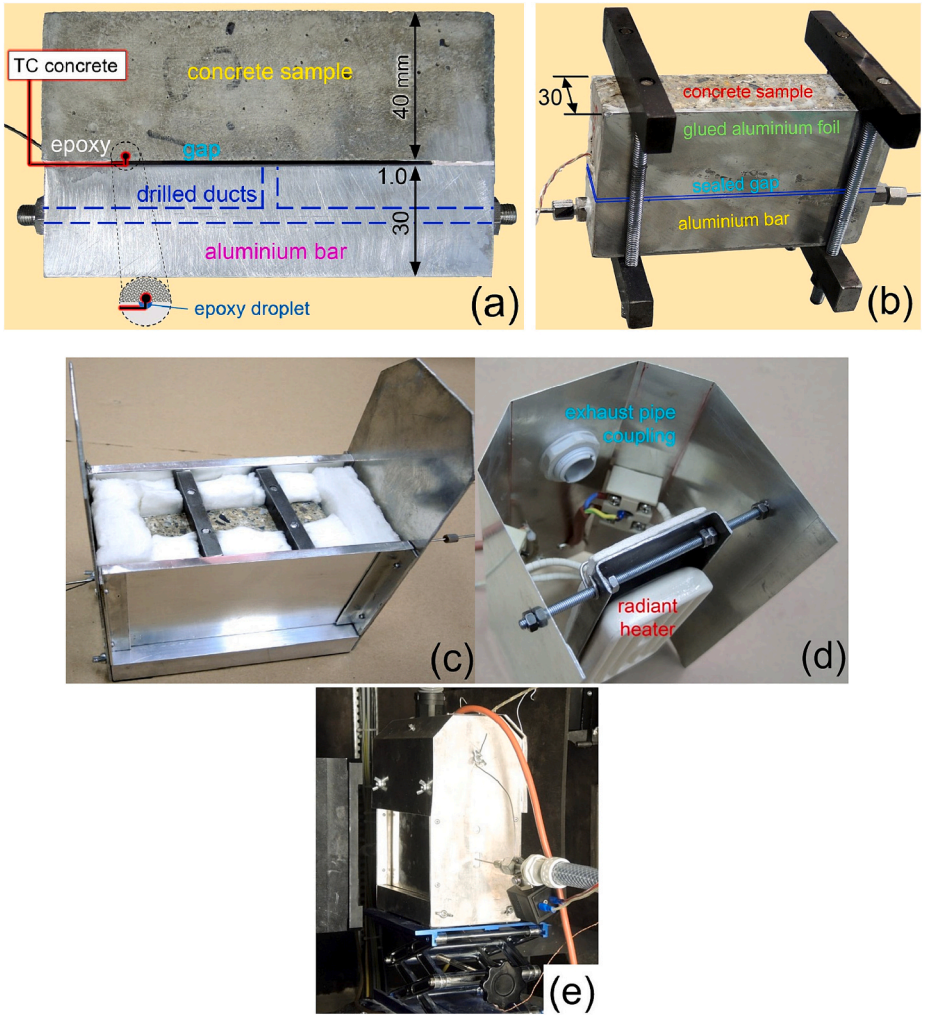

Fig. 6. Design sketch of the setup for the neutron radiography: (a), (b) Thin gap created between the concrete sample and the aluminium bar; (c) Sealed and tied sample before and after installation in the insulated aluminium holder; (d) Hood fitted with the radiant heater; (e) Installation of the complete setup in the beamline.

saturation is fairly high (e.g. 3 % of vaporized water from a 0.1 mm layer facing each side of a crack yields 4 kJ/m^2). The aim of the experimental campaign presented here is then to determine the absence or presence of this zone, and, in the latter case, characterize it.

Reducing the size of the involved region has a significant impact on the time scale of thermal and hygral transients. Heat conduction transients are ruled by Fourier's dimensionless time, which goes with 1/d^2 (where d is the distance through which conduction occurs). While heating rebars across a 30 mm cover may take one hour, moving heat within the influencing region would take a fraction of a second. Water movement is also expected to be considerably faster, because of both the reduced path distance and the steeper pressure gradients (i.e. higher

Table 1
Mix design and orientation of saw cut samples relative to the casting direction.

cement	500 kg/m^3	cement	500 kg/m^3
water (20 % by volume)	200 kg/m^3	water (20% by volume)	200 kg/m^3
w/c	0.4	w/c	0.4
siliceous aggregate (d = 6 mm) *Bolomey's grading curve, workability A = 12*	1693 kg/m^3	siliceous aggregate (d=6mm) *Bolomey's grading curve, workability A=12*	1693 kg/m^3
plasticizer (% of cement b.w.)	1 %	plasticizer (% of cement b.w.)	1%
age at testing	35 days	age at testing	35 days
compressive strength (100 mm cubes)	49 MPa	compressive strength (100mm cubes)	49 MPa

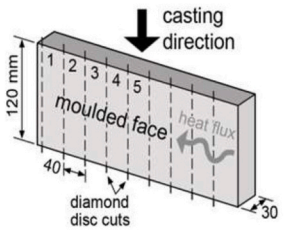

fluid velocity according to Darcy's law).

3. Experimental campaign

A specific setup was devised (Fig. 4) in order to confirm the ability of the influencing region to exhibit a fast thermal response under a sudden drop in pore pressure. One face of a concrete cylinder (diameter and height 100 mm) was sealed by glueing the rim of an aluminium plate with heat-resistant silicon (OTTOSEAL S17 by Otto Chemical). A small gap was left between the concrete face and the plate by inserting a spacer (a ring of 1 mm stainless steel wire, Fig. 4-b). A blind central hole and two radial ducts drilled in the plate allowed connecting the gap to a pressure sensor and a solenoid valve. The plate was secured with threaded ties to balance the thrust produced by vapour pressure (Fig. 4-c). The temperature of the concrete face was monitored with a thin shielded thermocouple (1 mm diameter) inserted in a sub-surface hole, indicatively 1 mm from the surface. After insulating the sample with ceramic fibre, one end of the concrete cylinder was heated utilizing a ceramic radiator. Both configurations in Fig. 4-a were checked. In principle, heating the sealing plate has the pros of faster response and no risk of vapour condensation in the ducts within the aluminium plate. On the other hand, a significant temperature difference develops between the plate and the sample (due to the thermal flux across the gap), the concrete face has a higher tendency to dry and the silicon undergoes more demanding operational conditions. In summary, the reversed layout with the sealed gap opposite to the heater proved more effective and reliable and was preferred thereafter.

The samples were some spare cylinders of ordinary concrete kept for several years in the laboratory environment. Despite the relatively low saturation and the lack of any lateral sealing, significant pressure was produced in the gap (≈ 1 MPa). Upon opening the solenoid valve the gauge pressure dropped to zero and sudden vaporization of moisture at the sealed surface was made possible (see Fig. 5). At the same time, a remarkable drop in temperature was observed (−90 °C), confirming that vaporization occurs at the price of a loss of thermal energy stored in the material. It has to be remarked that the response time of isolated shielded thermocouples to step temperature variations is not very fast (in the magnitude of some seconds). Then, the recorded rate of temperature change may have been partly reduced by the thermal inertia of the sensor. Nonetheless, the observed initial cooling rate was as high as 120 °C/s (see Fig. 5).

After 1.38 s from the opening of the valve, the temperature suddenly stopped decreasing and a sharp inversion of rate was exhibited (from −30 °C/s to +10 °C/s, see Fig. 5). This indicates the sudden end of water vaporization and the settling of the local thermal disturbance by plain heat conduction. The short time to settle (≈ 30 s) denoted a relatively thin disturbed layer and confirmed the above considerations about the expected size of the influencing region. For assessing the moisture migration engaged in this process, several techniques have been presented so far [27]. Among them, neutron imaging can detect even small moisture migrations thanks to the high attenuation produced by the nuclei of hydrogen atoms in water molecules [21,28–30]. Since the hygral process in the spalling event takes place in a very short time, high frame rates have to be achieved by scanning rather thin concrete samples under a high flux neutron beam. This latter requirement was fulfilled by taking advantage of testing facilities available at the Institut Laue Langevin (ILL) in Grenoble, France [26], which currently has the highest neutron flux in the world (about 3×10^8 neutrons per second per cm^2 at the instrument for our test). The aforementioned preliminary results on cylindrical samples were found to draw a coherent response of the material. Nevertheless, the cylindrical shape of the sample is not ideal for radiographic analysis, as the thickness of the sample varies along one axis of the detector. Therefore, conceptually analogous prismatic-shaped samples and setup were developed and tested. Notably, the direction orthogonal to the beam has been maximized to increase the amount of surface tested and thus the representativity of the results. In the direction parallel to the beam, a compromise was made between the representativity of the results and the penetration of neutrons to concrete. Based on experience, in fact, 30 mm was found to be a good compromise between reducing the beam attenuation and averaging the inherent material heterogeneity (Fig. 6). A relatively small aggregate size (6 mm) was also chosen for this latter purpose. This size is chosen as a compromise between the admissible thickness of concrete for the neutron opacity and the representativity of the samples. While this might affect the exact quantities at play we believe the fundamental processes, core of this work, to be maintained.

Contrary to tomographic 3D reconstructions [21], a single radiographic image reports the integral of the attenuation along the beam direction and then moisture variations across the specimen thickness should be minimized. For this reason, the opposite faces crossed by the beam were sealed with aluminium sheets (0.3 mm thickness) glued with heat-resistant epoxy resin (DP760 by 3 M). On the face to be submitted to pressure transients, a thin thermocouple with an exposed junction (0.3 mm wires) was glued directly onto the surface with an epoxy droplet. Then, an aluminium bar (30 × 30 mm) provided with drilled ducts and pipe connectors was glued with the same epoxy glue while interposing some spacers to leave a 1 mm gap (Fig. 6-a). The initial idea to leave the gap open (as reported in the Fig. 6-b) and then seal the sides just with the aluminium sheets proved to be prone to a blistering effect, due to the remarkable brittleness of the glue and stress concentration at the edges of the concrete prism. Hence, a thin rim of glue (about 3 mm) was applied along the major sides of the rod as well. It should be noted that the presence of a thermocouple can locally affect the material response (as noted for example in [20]), nevertheless, it should have a coherent effect among the tests. After mounting the restraint frames to balance the pressure developing in the gap, the sealed specimen was insulated with ceramic fibre and installed in the aluminium holder. The upper hood was fitted with the radiant heater and the exhaust pipe connector was then mounted on top of the holder. Finally, the whole box containing the sample was positioned in the neutron and X-ray imaging beamline D50 at ILL (Fig. 6-e).

The tests were performed on concrete samples batched according to

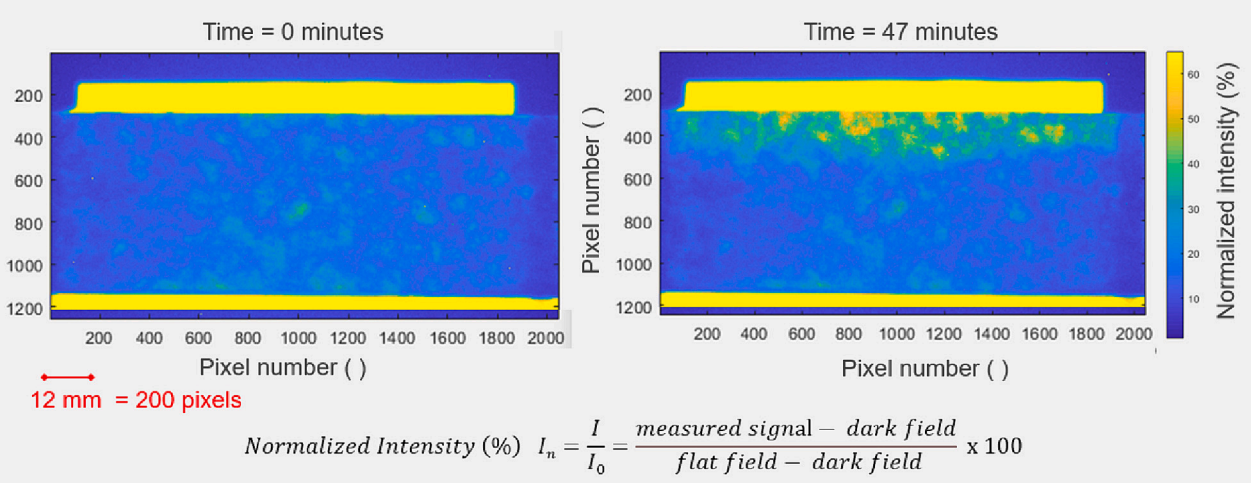

Fig. 7. Normalized radiography scans of the sample at the beginning and 47 min after heating from the top side.

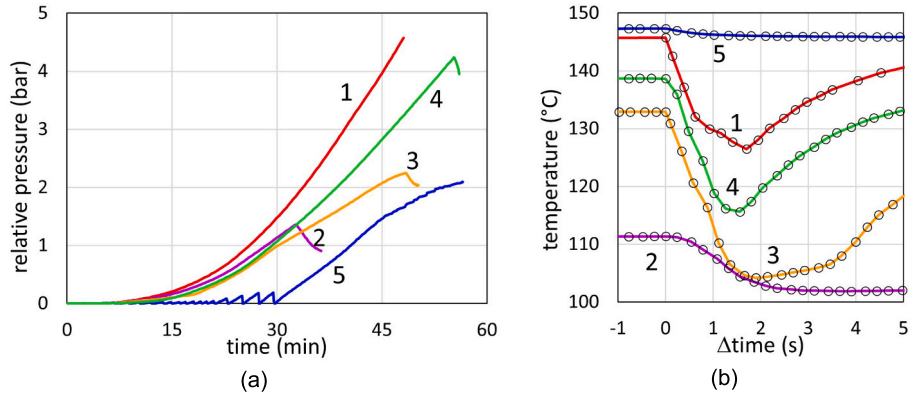

Fig. 8. (a) Pressure trends preceding the opening of the valve and (b) Temperature drops following it.

Table 2
Reference analysis parameters (the values are within the typical ranges reported for high-performance concrete [36]).

Reference scenario parameters (close to experiment)			
Material properties		Initial condition	
porosity (−)	0.103	temperature (°C)	160
convection coefficient	0.95	initial gas pressure (MPa)	0.4
intrinsic permeability (m^2)	1.5e-17	initial relative humidity (−)	0.7
vapour diffusivity (m^2/s)	2.85e-5	external humidity (−)	0.5
specific heat (J/kg.°C)	910		

the mix design of Table 1. Rectangular slabs were cast parallel to their plane as sketched in the figure in the inset of Table 1, demolded after one day and cured in water for one week. Curing continued in the laboratory environment till the time of testing. The samples were 40 mm high prisms obtained by cutting the slabs with the diamond disc. The moulded faces were sealed with 0.3 mm aluminium sheets, whereas the sawcut faces were submitted to the hygral transients. The underlying idea was to better replicate the material texture typical of a natural crack. Right before testing, the capillary pipe connected to the pressure sensor was filled with silicon oil and the ducts drilled in the aluminium bar were partly filled with water, so as to limit moisture loss from the region of interest during the preliminary heating stage.

The tests were run by switching on the heater at full power until the target temperature of 500 °C was reached by the built-in control thermocouple of the radiator. Pressure and temperature in the sealed gap opposite to the heated face were continuously monitored and neutron images were taken at regular time intervals (about 90 s). When a change in the increasing rate of pressure was recognized, denoting the impending attainment of a pressure peak (normally after 30–60 min heating), the maximum image acquisition rate was set (33 frames/s) and the solenoid valve was opened while recording temperature and pressure at the maximum available rate (4 samples/s). At this frame rate, the image resolution was 0.09 mm/pixel, which is still adequate to monitor the shallow drying process occurring next to the sealed gap.

4. Results and discussion

The five samples documented in the following are the ones tested in-operando at ILL. Nevertheless, another two tests were performed beforehand to characterize the response. Four of the five tests studied are a-priori identical and are performed on a nominally identical material, albeit there is an intrinsic variability, linked to the sealing conditions and local heterogeneities. Notably, the accumulated pressure before the release of the valve was slightly different, resulting in quantitative differences in the pressure drop. This actually helps shed light on the interplay between pressure drop and moisture migration.

The fifth sample was instead pre-dried by opening the valve multiple times so as to assess the effect of different moisture content. The corresponding pressure and temperature plots in Fig. 8 are similar to the ones obtained in the preliminary tests in Fig. 5. Nevertheless, the tests performed in the neutron beamline show slightly lower pressure peaks (0.1–0.5 MPa), which occur at lower temperatures, possibly because of

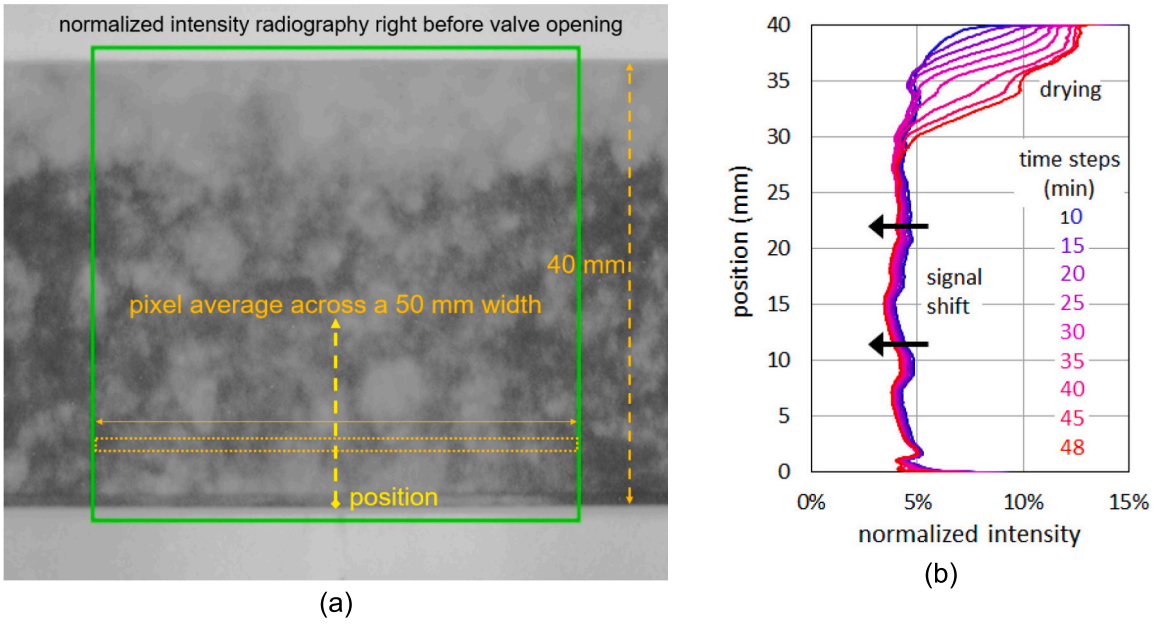

Fig. 9. (a) NR image of sample #3 right before valve opening and (b) Profiles of the normalized intensity averaged along horizontal lines in the highlighted region of interest.

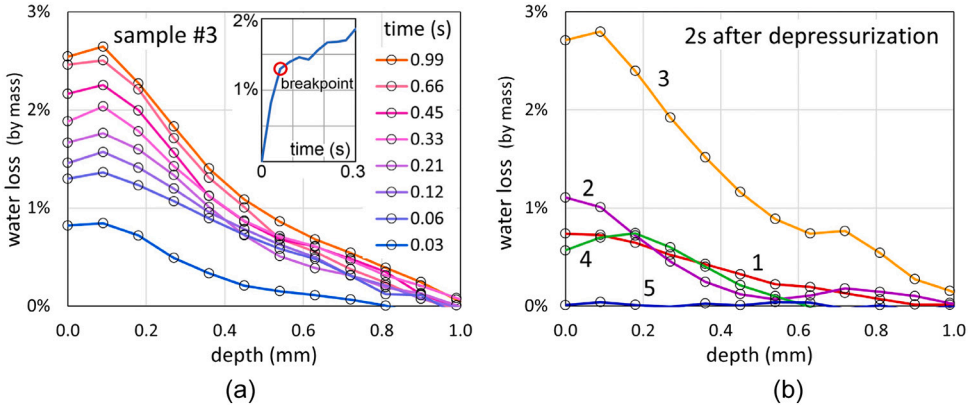

Fig. 10. (a) Evolution of moisture profiles during the fast transient following the valve opening in #3 and (b) Final profiles observed in the first 5 tests.

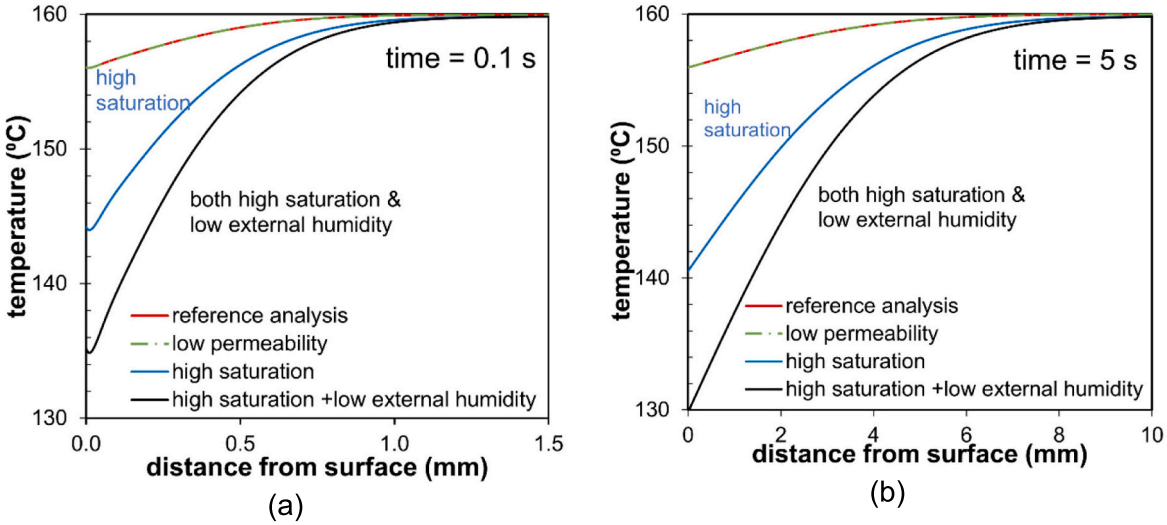

Fig. 11. Temperature drop in (a) 0.1 and (b) 5 s after releasing pressure.

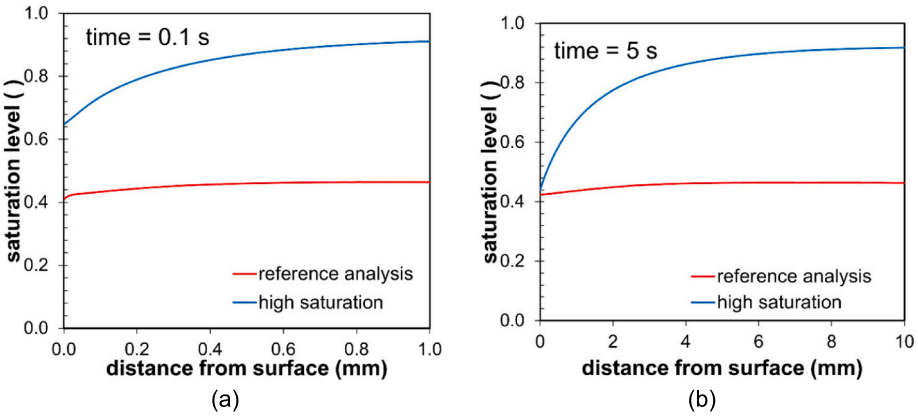

Fig. 12. Saturation level in (a) 0.1 and (b) 5 s after releasing pressure on the left boundary.

the different sealing conditions, leading to minor vapour leakages in the preliminary stage of the test (e.g. sample #2). Accordingly, the temperature drops at the valve opening were also less pronounced (up to −30 °C) and characterized by milder transients, with an initial quasi-linear trend (−20 °C/s) and the attainment of the minimum temperature in about 2 s. In this case, the faster response of the exposed junction thermocouples and the relatively slower process allowed a reliable monitoring of the transient. In one test (sample #5), the valve was opened several times during the heating stage, to allow partial drying of the sample. Despite the significant pressure reached afterwards, the valve opening produced a very weak thermal transient (proof that the Joule-Thomson effect plays a negligible role in the measured temperature drops). It should also be noted that in samples #2 and #4, it was possible to re-pressurize the gap (up to 0.10–0.15 MPa pressure) in the same test run, but no thermal perturbation was induced upon the second valve opening.

In the neutron radiographic images, the drying front was observed to penetrate 10–15 mm from the top face during the preliminary heating phase, as is denoted by the lighter grey tone in Fig. 9-a. For each pixel, the normalized neutron attenuation $I_n = I / I_0$ was computed by subtracting from the measured signal the background noise of the camera (dark field) and dividing by the unencumbered beam intensity (flat field I_0), also corrected by the dark field. A representative final, corrected image, as well as the normalisation operation are reported in Fig. 7. The ensuing normalized intensity profiles of the neutron attenuation are shown as a function of the distance from the bottom sealed face in Fig. 9-b (values are averaged across a 50 mm width to reduce the effect of aggregates). In this plot, the attenuation of the aluminium casing and the insulating ceramic (measured to be 10 % in the unencumbered area above the sample) was subtracted so as to isolate the role of water and concrete.

The Beer-Lambert law allows us to estimate the strong beam attenuation entailed by the 30 mm thick sample:

$$I_n = I/I_0 = exp\left[-\left(\Sigma_{water}\cdot\tau_{water} + \Sigma_{conc}\cdot\tau_{conc}\right)\right] = exp\left[-\left(0.35\cdot 6 + 0.065\cdot 30\right)\right] = 1.7\% \quad (1)$$

where Σ_{water} and Σ_{conc} are the attenuation coefficients of water and dry concrete for the median wavelength of the beamline, and τ_{water} and τ_{conc} their thicknesses. The concrete thickness can be directly measured, and the corresponding equivalent water thickness can be deduced by the mix design of Table 1. As for the attenuation coefficients, they can be calculated from the literature [31] or online databases (e.g., the one from the International Agency for Atomic Energy -IAEA- as https://www-nds.iaea.org/exfor/endf.htm).

In fact, the initial beam intensity observed in the core of the sample is 4.4 %, which is significantly more than what is indicated by the exponential attenuation law. Moreover, a slight shift to lower values is observed in the same region during the heating stage. Both effects can be explained by the spurious contribution of scattering. Given the significant water content in the sample, neutrons interacting with hydrogen nuclei of water are randomly dispersed away from their original straight trajectory and contribute to the intensity detected by the surrounding pixels of the detector. As the heated part of the sample dries, this spurious flux is reduced, inducing an overall signal decline in the neighbouring areas.

To estimate this contribution, the parametric scattering correction model was applied on the results (see Appendix A). This model, proposed in [32], was calibrated to the parameters of the NeXT beamline at ILL, following the calibration tests on a water-filled wedge-shaped box reported in [33].

To study the effects of the sudden depressurization on the local moisture content next to the bottom sealed face, the last 10 images acquired before the valve opening were averaged and used as a reference. Based on the above discussed scattering corrections, the mass loss of water with respect to the mass of concrete for each pixel can be computed as:

$$\text{mass loss}\,(\%) = \rho_{water}/\Sigma_{water}\cdot\left[ln\left(I_n - I_{scatt}\right) - ln\left(I_{n,ref} - I_{scatt}\right)\right]/\left(\tau_{conc}\cdot\rho_{conc}\right)\times 100 \quad (2)$$

where $\Sigma_{water} = 0.35\ mm^{-1}$ is the attenuation coefficient of water

$\tau_{conc} = 30$ mm is the sample thickness

$\rho_{water} / \rho_{conc} = 1 / 2.4$ is the ratio of water and concrete densities

$I_{scatt} = 2$ % is the contribution of scattering at the bottom face after pre-heating (Fig. 13-b)

The mass loss profiles at increasing distance from the depressurized interface and their evolution with time are reported in Fig. 10-a. A drying profile can be recognized already in the first frames, a few hundredths of a second after the valve opening. The rather small temperature drop observed in this transient (−29 °C, see Fig. 8), suggests a modest amount of energy released as stored sensible heat. This energy should be able to vaporize 1.2 % of water by mass (specific heat of concrete = 920 J/kg°C, latent heat of vaporization = 2200 kJ/kg at 120 °C). Heat conduction from the deeper layers is then required to proceed, which also explains the progressive slowing down of the process, which essentially stops within a couple of seconds. Qualitatively analogous results were also obtained in the other tests (Fig. 10-b).

This analysis corroborates the idea that the quick temperature drop following the sudden depressurization of hot moist concrete is caused by the semi-instantaneous vaporization of a share of the water available in the pores. It should be noted that larger magnitudes of temperature and moisture variations and faster times are expected in typical conditions leading to explosive spalling.

5. Numerical analysis

The main focus of this work is understanding the fast transient entailed by the opening of a fracture. While the main novelty of the experiments is to shed light on the evolution of the moisture distribution, we also measure the spatial gradients of temperature drop. This is closely related to the thermal energy absorbed by water vaporization.

A thermo-hydro-mechanical model was adopted not only to corroborate experimental observations of the fast transient, but also to identify which parameters govern the process. The model is based on the hybrid mixture theory first proposed by Lewis and Schrefler [34]. Here the cement-based material is described as a partially saturated porous medium comprising a solid skeleton with interconnected porosity filled by capillary water, vapour and dry air. The phenomena currently believed to lead to the high-temperature behaviour are explicitly described in the model (e.g. temperature-dependent properties, the release of bound water, and phase changes and Darcy's law).

For the heat and mass transfer in porous media, the numerical model [35] is based on the general TCAT (Thermodynamically Constrained Average Theory) framework. In brief, the solid matrix and the fluid in the pores are averaged in a representative volume and the conservation equations of mass, energy and momentum are formulated at the continuum level. This approach is well established not only for building materials but also in various other fields such as food drying, fuel cells, packed bed reactors, groundwater and oil/gas exploitation. For concrete at high temperatures, the fluid in the pores is considered a two-phase fluid consisting of free water (capillary and adsorbed) and gas (vapour and dry air). Fluid transport is then modelled by a generalized Darcy's law and by Fick's law for gas diffusion. The general approach to modelling non-equilibrium isotherm mass transfer processes in an open porous medium is to start from a set of balance equations governing the mass time evolution of fluids filling the porous network and their exchange with the surrounding medium. These balance equations are supplemented with an appropriate set of constitutive relationships which permit to reduce the number of independent state variables that control the physical process in concern such as dehydration, material properties evolution with temperature and pressure, etc. The reader is referred to research by Dal Pont, Durand and Schrefler for their detailed expressions [35].

Material properties are summarized in Table 2. Since the concrete specimens have not been fully characterized, some standard parameters for normal-grade concrete (i.e. compressive strength of concrete after 28 days = 49 MPa) have been adopted to describe the transport properties (mostly porosity and intrinsic permeability [36]). Nevertheless, in some works the intrinsic permeability is reported to be one or two orders of magnitude lower (e.g. [37]), thus justifying the parametric study reported in scenario 2 (see Table 2). Regarding initial and boundary conditions imposed in the model, the average relative humidity of the beamline was previously assessed as ~30 % [35], but can be significantly higher since the hall is not climatised. However, the assigned relative humidity on the sample is higher (0.7) due to the presence of the moist gap. Initial and boundary conditions are also given in Table 2. The initial temperature, as well as the initial gas pressure, are equivalent to the experimental ones before releasing the pressure, i.e., T=160 °C and Pg = 0.4 MPa. The numerical analysis is performed on the first 25 mm of concrete, and its results are reported in Fig. 11. The equations are solved through a finite element simulation, with an in-house developed constitutive routine, implemented within Cast3m [35], discretized by 1280 elements (element size from 0.005 mm to 0.05 mm, the smaller size being closer to the depressurized interface). Regarding external humidity, it depends on the location and season of testing. It should be noted that because of the non-smooth boundary conditions, numerical instabilities are likely to occur. To address this, a time step of 0.01 s was adopted. Then, after assigning the reference scenario including material properties and the initial condition, a parametric analysis was performed not only to approach the observed behaviour but also to investigate the influence of different parameters on the results. In the second scenario, the effect of low permeability on the results is assessed which can give a hint to understanding the conditions in higher grades of concrete mixes [37]. Scenarios 4 and 3 are identical except for the external humidity, which is dryer in the latter case.

In summary, four scenarios were tested:

1. Reference scenario with the parameters detailed in Table 2.
2. Decrease of intrinsic permeability to 1.5e-19 m^2
3. Increase of initial moisture content (saturation level to 92 %)
4. Increase of initial moisture content (saturation level to 92 %) and external RH to 25 %

In the reference scenario, which emulates the experimental conditions without considering the possible moisture clog phenomenon in the preheating phase, just a minor temperature drop is observed. In other words, little water vaporization is induced by the pressure release in this condition. Of course, as time progresses the temperature gradient propagates deeper in the sample. This temperature drop is far from the experimentally observed one, which is only captured qualitatively. The model is designed for quasi-static conditions and was shown to be able to capture the evolution of the conditions leading to the development of the virtual crack. These observations suggest that the model should be extended to include fast transients, notably improving the description of the energy balance. The change of permeability, as expected, has very limited influence on the response. Increasing the internal water content rises the temperature drop to 30 °C, closer to the experimentally observed one. This effect is exacerbated if the external humidity is lower.

To compare the results with neutron radiography ones, the trends of saturation for the two cases of reference and high initial moisture are presented in Fig. 12. In the reference analysis, the initial moisture is a typical value (relative humidity of 70 %). However, higher initial moisture in the moment of release can be more representative of the real case in the experimental test and in a spalling event due to the moisture transport from the heated boundary and accumulation in the colder zone (moisture clog). In the case of a higher saturation level, a higher amount of water is lost in the very superficial layer next to the boundary. This water should be vaporized and fed into the incipient crack, whose propagation is boosted by the ensuing pressure, leading to the violent expulsion of the concrete cover. As it was previously mentioned, water inside the pores plays a crucial role in converting the huge thermal energy available in the heated concrete into kinetic energy and this role is more pronounced when there is a rather moist region next to an initiated crack. All these results were strongly dependent on the level of initial pressure and initial moisture and on the boundary conditions. Due to high nonlinearity in the equations, higher initial pressure would give rather unstable and non-converging results. Hence, the actual behaviour of concrete next to the gap might be even more severe when gas pressure is higher and mass transport is potentially facilitated according to Darcy's law. It should be noted that the curves in Fig. 12 qualitatively match the experimental responses in Fig. 10. Notably the process tends to focus mostly in the first millimeter during the first second and then slowly propagates deeper in the concrete.

6. Concluding remarks

In this paper, the quick thermal and hygral transients occurring upon depressurization of an internal interface in hot moist concrete have been addressed as a possible explanation for the explosive nature of spalling in fire. A bespoke test was designed to study rapid moisture migration in real-time through Neutron Radiography. A thermo-hydro-mechanical model was adopted and validated against these experimental observations to pinpoint the key parameters influencing the fast transient phenomenon.

The main conclusions are:

- A sudden temperature drop follows the depressurization of pores. A decrease of 30–90 °C and a cooling rate of 20–120 °C/s were observed in laboratory tests starting from relatively low initial pressures and temperatures (up to 1 MPa at 200 °C). Higher drops are expected in realistic fire conditions.
- Fast neutron radiography images confirm that during these transients a fraction of moisture depending on the local temperature and saturation is quickly vaporized within a thin layer (about 1 mm thickness) facing the depressurized interface. In this region, the first variation in moisture content is noticeable already after 0.03 s.
- When considering a real explosive spalling event, the issue is exacerbated, since the heat mobilized by cooling a unit volume of concrete by 100 °C is three orders of magnitude higher than the expected elastic energy due to thermal strain [15]. A share of this thermal energy can quickly vaporize the liquid water in a very thin layer facing each face of an opening crack. The layer thickness allows fast vapour migration since the diffusion time goes with the path length squared. The corresponding work of the adiabatic expansion is able to accelerate the fractured splinter to the remarkable velocities documented in real fire tests, the magnitude depending on the initial saturation of the pores.
- The temperature drop occurs also in the numerical model. The saturation gradient starts at the depressurized face, and then it penetrates to deeper layers. The initial saturation level and the external relative humidity have the highest impact on the severity of this temperature drop. In the most favourable conditions, a very fast transient develops, coherent with the highly dynamic process of explosive spalling.

In future works, the development of a setup allowing the generation of a real crack is needed to be fully representative. While convenient for a proof-of-concept experiment, the artificial crack retained in this study is not representative of the intrinsic complexity of the initiation and propagation of a real fissure. It is also worth noting that the sealing limits the maximum attainable pressure, which would not be the case for a real crack. Nevertheless, we believe the trends observed to be representative of the process.

These results suggest the need for renewed attention in both experimental and numerical studies on the role of the fast thermo-hygral transient involved by the explosive spalling phenomenon. Models are very good at reproducing quasi-static conditions (moisture transport) thus describing the condition that will favour spalling, but they provide just a qualitative representation of the fast transient, thus suggesting that an effort should be made in this direction.

CRediT authorship contribution statement

Roberto Felicetti: Writing – review & editing, Writing – original draft, Visualization, Validation, Supervision, Software, Resources, Project administration, Methodology, Investigation, Funding acquisition, Formal analysis, Data curation, Conceptualization. **Ramin Yarmohammadian:** Writing – review & editing, Writing – original draft, Visualization, Validation, Software, Resources, Methodology, Investigation, Formal analysis, Data curation, Conceptualization. **Stefano Dal Pont:** Writing – review & editing, Writing – original draft, Visualization, Validation, Supervision, Software, Resources, Project administration, Methodology, Investigation, Funding acquisition, Formal analysis, Data curation, Conceptualization. **Alessandro Tengattini:** Writing – review & editing, Writing – original draft, Visualization, Validation, Supervision, Software, Resources, Methodology, Investigation, Formal analysis, Data curation, Conceptualization.

Declaration of competing interest

The authors declare that they have no known competing financial interests or personal relationships that could have appeared to influence the work reported in this paper.

Data availability

Data will be made available on request.

Acknowledgement

The authors acknowledge the support of the French Agence Nationale de la Recherche (ANR) (project MULTI-FIRE ANR-23-CE51-0001-01). We wish to acknowledge the feedback of the reviewers that has helped substantially improve the quality of the paper.

Appendix A. Correction of neutron scattering

To assess the contribution of neutron scattering, we employed the parametric scattering correction model, as outlined in [32]. This model has been specifically calibrated to the parameters of the NeXT beamline at ILL. The calibration process involved rigorous tests on a water-filled wedge-shaped box, as detailed in [33].

As shown in Fig. 13-a, the model fits well with the significant increase in the detected beam intensity with respect to the uncollided share predicted by the Beer-Lambert law. In our geometry (small 40 mm sample height compared to the 105 mm distance from the detector) the assessed contribution of scattering is relatively uniform (black solid plot in Fig. 13-b). The magnitude of the scattered radiation (2.6 % on average) is consistent with the observed difference between experimental and predicted intensities. This estimate also coincides with the intensity detected behind the neutron shield installed around the region of interest of the test setup (a 5 mm thick boron carbide layer whose neutron attenuation exceeds 99.9 %).

As concerns the gradual shift of the intensity profiles in the core region of the sample, a notional full drying of a 7 mm surface layer (a step function equivalent in area to the final sigmoidal profile in Fig. 9, to the right) was also considered in the model. The magnitude and trend of the scattering reduction (black dashed plot in Fig. 13-b) are consistent with the observed tendency.

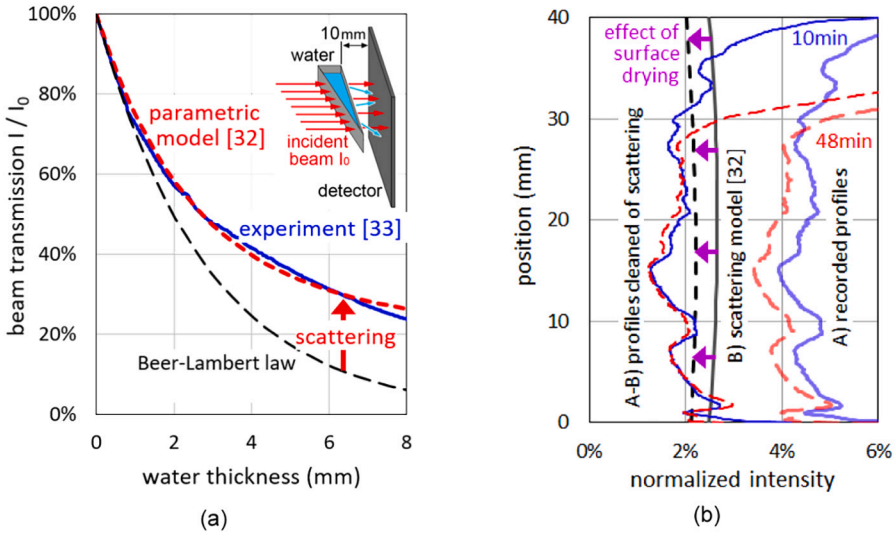

Fig. 13. Effect of scattering according to the parametric model: (a) Beam intensification in case of linearly increasing water thickness and (b) Intensity reduction due to surface drying in sample #3.

This scattering contribution can be then subtracted from the original normalized intensities of moist and dry concrete, thus determining their actual neutron attenuations. The mean attenuation in the moist core of the sample (1.8 % at any stage of the preliminary heating) now matches the indication of the Beer-Lambert law (Eq. (3)). The comparison against the larger intensity reached at top face in the end of the preliminary heating process (11 %) allows computing the variation in water content as:

$$ln\left(I_{n,wet}\right) - ln\left(I_{n,dry}\right) = -\left(\Sigma_{water}\cdot\tau_{water\_ini} + \Sigma_{conc}\cdot\tau_{conc}\right) + \left(\Sigma_{water}\cdot\tau_{water\_fin} + \Sigma_{conc}\cdot\tau_{conc}\right) = \Sigma_{water}\cdot\Delta\tau_{water} \quad (3)$$

$$\Delta\tau_{water} = \ln(0.018/0.11) \,/\, 0.35\ mm^{-1} = -5.2\ mm$$

As expected, this indicates a substantial drying, close to the original water content of the mix, estimated to be 6 mm in thickness. It should be noted that this is a sizably larger figure than it would have been obtained with no correction for scattering (−3.0 mm).

References

[1] J.-C. Liu, K.H. Tan, Y. Yao, A new perspective on nature of fire-induced spalling in concrete, Constr. Build. Mater. 184 (2018) 581–590, https://doi.org/10.1016/j.conbuildmat.2018.06.204.

[2] Waraich E. Klingsch, Explosive spalling of concrete in fire, in: Brisk Bin. Robust Invariant Scalable Keypoints, 2009, pp. 12–19, https://doi.org/10.3929/ethz-a-010025751.

[3] D. Gawin, C. Alonso, C. Andrade, C.E. Majorana, F. Pesavento, Effect of damage on permeability and hygro-thermal behaviour of HPCs at elevated temperatures: part 1. Experimental results, Comput. Concr. 2 (2005) 189–202, https://doi.org/10.12989/cac.2005.2.3.189.

[4] J. Zhao, J.J. Zheng, G.F. Peng, K. Van Breugel, A meso-level investigation into the explosive spalling mechanism of high-performance concrete under fire exposure, Cem. Concr. Res. 65 (2014) 64–75, https://doi.org/10.1016/j.cemconres.2014.07.010.

[5] Y. Fu, L. Li, Study on mechanism of thermal spalling in concrete exposed to elevated temperatures, Mater. Struct. Constr. 44 (2011) 361–376, https://doi.org/10.1617/s11527-010-9632-6.

[6] H. Carré, P. Pimienta, C. La Borderie, F. Pereira, J.C. Mindeguia, Effect of compressive loading on the risk of spalling, MATEC Web Conf. 6 (2013) 1–9, https://doi.org/10.1051/matecconf/20130601007.

[7] H.L. Zhang, C.T. Davie, A numerical investigation of the influence of pore pressures and thermally induced stresses for spalling of concrete exposed to elevated temperatures, Fire Saf. J. 59 (2013) 102–110, https://doi.org/10.1016/j.firesaf.2013.03.019.

[8] Z.P. Bažant, G. Cusatis, Concrete creep at high temperature and its interaction with fracture: recent progress, in: Concreep 7 Conf. Creep, Shrinkage Durab. Concr. Concr. Struct, 2005, pp. 449–460.

[9] M.B. Dwaikat, V.K.R. Kodur, Hydrothermal model for predicting fire-induced spalling in concrete structural systems, Fire Saf. J. 44 (2009) 425–434, https://doi.org/10.1016/j.firesaf.2008.09.001.

[10] M. Ozawa, H. Morimoto, Effects of various fibres on high-temperature spalling in high-performance concrete, Constr. Build. Mater. 71 (2014) 83–92, https://doi.org/10.1016/j.conbuildmat.2014.07.068.

[11] P. Kalifa, F.D. Menneteau, D. Quenard, Spalling and pore pressure in HPC at high temperatures, Cem. Concr. Res. 30 (2000) 1915–1927, https://doi.org/10.1016/S0008-8846(00)00384-7.

[12] P. Kalifa, G. Chéné, C. Gallé, High-temperature behaviour of HPC with polypropylene fibres, Cem. Concr. Res. 31 (2001) 1487–1499, https://doi.org/10.1016/s0008-8846(01)00596-8.

[13] S. Dal Pont, H. Colina, A. Dupas, A. Ehrlacher, An experimental relationship between complete liquid saturation and violent damage in concrete submitted to high temperature, Mag. Concr. Res. 57 (2005) 455–461, https://doi.org/10.1680/macr.2005.57.8.455.

[14] T. Tanibe, M. Ozawa, R. Kamata, K. Rokugo, Steel ring-based restraint of HSC explosive spalling in high temperature environments, J. Struct. Fire Eng. 5 (2014) 239–250, https://doi.org/10.1260/2040-2317.5.3.239.

[15] D. Gawin, F. Pesavento, B.A. Schrefler, Towards prediction of the thermal spalling risk through a multi-phase porous media model of concrete, Comput. Methods Appl. Mech. Eng. 195 (2006) 5707–5729, https://doi.org/10.1016/j.cma.2005.10.021.

[16] M. Zeiml, R. Lackner, H.A. Mang, Experimental insight into spalling behavior of concrete tunnel linings under fire loading, Acta Geotech. 3 (2008) 295–308, https://doi.org/10.1007/s11440-008-0069-9.

[17] M. Ozawa, S. Uchida, T. Kamada, H. Morimoto, Study of mechanisms of explosive spalling in high-strength concrete at high temperatures using acoustic emission, Constr. Build. Mater. 37 (2012) 621–628, https://doi.org/10.1016/J.CONBUILDMAT.2012.06.070.

[18] R. Felicetti, F. Lo Monte, P. Pimienta, A new test method to study the influence of pore pressure on fracture behaviour of concrete during heating, Cem. Concr. Res. 94 (2017) 13–23, https://doi.org/10.1016/j.cemconres.2017.01.002.

[19] F. Lo Monte, R. Felicetti, M.J. Miah, The influence of pore pressure on fracture behaviour of normal-strength and high-performance concretes at high temperature, Cem. Concr. Compos. 104 (2019) 103388, https://doi.org/10.1016/j.cemconcomp.2019.103388.

[20] D. Dauti, A. Tengattini, S.D. Pont, N. Toropovs, M. Briffaut, B. Weber, Some observations on testing conditions of high-temperature experiments on concrete: an insight from neutron tomography, Transp. Porous Media 132 (2020) 299–310, https://doi.org/10.1007/s11242-020-01392-2.

[21] D. Dauti, A. Tengattini, S. Dal Pont, N. Toropovs, M. Briffaut, B. Weber, Analysis of moisture migration in concrete at high temperature through in-situ neutron tomography, Cem. Concr. Res. 111 (2018) 41–55, https://doi.org/10.1016/j.cemconres.2018.06.010.

[22] A. Tengattini, S. Dal Pont, H. Cheikh Sleiman, F. Kisuka, M. Briffaut, Quantification of evolving moisture profiles in concrete samples subjected to temperature gradient by means of rapid neutron tomography: influence of boundary conditions, hygro-thermal loading history and spalling mitigation additives, Strain 56 (2020) 1–14, https://doi.org/10.1111/str.12371.

[23] M. Moreira, S.D. Pont, A. Tengattini, V. Pandolfelli, Heating rate effect on the moisture clog while drying refractory castables: a neutron tomography perspective, J. Am. Ceram. Soc. 106 (2022) 1706–1715, https://doi.org/10.1111/jace.18902.
[24] D.P. Bentz, Fibers, percolation, and spalling of high performance concrete, ACI Mater. J. (2000). https://www.researchgate.net/publication/234155149 (accessed October 26, 2023).
[25] R. Felicetti, R. Yarmohammadian, S.D. Pont, A. Tengattini, Flash vaporization next to an opening crack: a possible explanation of the explosive nature of concrete spalling, in: 6th International Workshop on Concrete Spalling Due to Fire Exposure, Sheffield, 2019, pp. 237–247.
[26] A. Tengattini, N. Lenoir, E. Andò, B. Giroud, D. Atkins, J. Beaucour, G. Viggiani, NeXT-Grenoble, the neutron and X-ray tomograph in Grenoble, Nucl. Instruments Methods Phys. Res. Sect. A Accel. Spectrometers, Detect. Assoc. Equip. 968 (2020) 163939, https://doi.org/10.1016/j.nima.2020.163939.
[27] R.T.C.-M. Rilem, Methods of Measuring Moisture in Building Materials and Structures, 1st ed, Springer Cham, 2018, https://doi.org/10.1007/978-3-319-74231-1.
[28] T. Kannangara, P. Joseph, S. Fragomeni, M. Guerrieri, Existing theories of concrete spalling and test methods relating to moisture migration patterns upon exposure to elevated temperatures – a review, Case Stud. Constr. Mater. 16 (2022) e01111, https://doi.org/10.1016/j.cscm.2022.e01111.
[29] C. Hartnig, I. Manke, Measurement methods | structural properties: neutron and synchrotron imaging, in-situ for water visualization, Encycl. Electrochem. Power Sour. (2009) 738–757, https://doi.org/10.1016/B978-044452745-5.00078-2.
[30] R. Satija, D.L. Jacobson, M. Arif, S.A. Werner, In situ neutron imaging technique for evaluation of water management systems in operating PEM fuel cells, J. Power Sources 129 (2004) 238–245, https://doi.org/10.1016/j.jpowsour.2003.11.068.
[31] H. Börner, J. Brown, C.J. Carlile, R. Cubitt, R. Currat, A.J. Dianoux, B. Farago, A. Hewat, J. Kulda, E. Lelièvre-Berna, G. McIntyre, S.A. Mason, R.P. May, A. Oed, J.R. Stewart, F. Tasset, J. Tribolet, R.S. Eccleston, M. Johnson, C.C. Wilson-ISIS, G. Lander, H. Rauch, W. Waschkowski, A. Mader, Neutron Data Booklet. www.ill.fr, 2003 (accessed February 9, 2024).
[32] R. Hassanein, E. Lehmann, P. Vontobel, Methods of scattering corrections for quantitative neutron radiography, Nucl. Instruments Methods Phys. Res. Sect. A Accel. Spectrometers, Detect. Assoc. Equip. 542 (2005) 353–360, https://doi.org/10.1016/J.NIMA.2005.01.161.
[33] E. Stavropoulou, E. Andò, A. Tengattini, M. Briffaut, F. Dufour, D. Atkins, G. Armand, Liquid water uptake in unconfined Callovo Oxfordian clay-rock studied with neutron and X-ray imaging, Acta Geotech. 14 (2019) 19–33, https://doi.org/10.1007/S11440-018-0639-4/FIGURES/13.
[34] R. Lewis, B. Schrefler, The Finite Element Method in the Static and Dynamic Deformation and Consolidation in Porous Media, 1998.
[35] S. Dal Pont, S. Durand, B.A. Schrefler, A multiphase thermo-hydro-mechanical model for concrete at high temperatures-finite element implementation and validation under LOCA load, Nucl. Eng. Des. 237 (2007) 2137–2150, https://doi.org/10.1016/j.nucengdes.2007.03.047.
[36] S. Dal Pont, B.A. Schrefler, A. Ehrlacher, Intrinsic permeability evolution in high temperature concrete: an experimental and numerical analysis, Transp. Porous Media 60 (2005) 43–74, https://doi.org/10.1007/S11242-004-3252-Y/METRICS.
[37] V. Picandet, A. Khelidj, G. Bastian, G.B. Effect, Axial compressive damage on gas permeability of ordinary and high performance concrete, Cem. Concr. Res. (2001) 31, https://doi.org/10.1016/S0008-8846(01)00546-4ï.